

RESEARCH ARTICLE

Matrix stiffness regulates α -TAT1-mediated acetylation of α -tubulin and promotes silica-induced epithelial–mesenchymal transition via DNA damage

Gengxu Li^{1,*}, Si Chen^{2,*}, Yi Zhang¹, Hong Xu³, Dingjie Xu⁴, Zhongqiu Wei¹, Xuemin Gao³, Wenchen Cai³, Na Mao³, Lijuan Zhang³, Shumin Li¹, Fang Yang³, Heliang Liu³ and Shifeng Li^{3,†}

ABSTRACT

Silicosis is characterized by silica exposure-induced lung interstitial fibrosis and formation of silicotic nodules, resulting in lung stiffening. The acetylation of microtubules mediated by α -tubulin N-acetyltransferase 1 (α -TAT1) is a posttranslational modification that promotes microtubule stability in response to mechanical stimulation. α -TAT1 and downstream acetylated α -tubulin (Ac- α -Tub) are decreased in silicosis, promoting the epithelial–mesenchymal transition (EMT); however, the underlying mechanisms are unknown. We found that silica, matrix stiffening or their combination triggered Ac- α -Tub downregulation in alveolar epithelial cells, followed by DNA damage and replication stress. α -TAT1 elevated Ac- α -Tub to limit replication stress and the EMT via trafficking of p53-binding protein 1 (53BP1, also known as TP53BP1). The results provide evidence that α -TAT1 and Ac- α -Tub inhibit the EMT and silicosis fibrosis by preventing 53BP1 mislocalization and relieving DNA damage. This study provides insight into how the cell cycle is regulated during the EMT and why the decrease in α -TAT1 and Ac- α -Tub promotes silicosis fibrosis.

This article has an associated First Person interview with the first authors of the paper.

KEY WORDS: α -tubulin N-acetyltransferase 1, Acetylated α -tubulin, DNA damage, Epithelial–mesenchymal transition, Silicosis

INTRODUCTION

Silica (SiO₂) exposure is a common risk factor for silicosis, and new cases of severe SiO₂ toxicity are still being reported (Cohen et al., 2016). The mode of action for SiO₂-induced silicosis implicates inflammation and reactive oxygen species. We and others have reported that SiO₂ particles induce accumulation of DNA double-strand breaks (DSBs) in type II alveolar epithelial cells (AECs)

(Shifeng et al., 2019; Zheng et al., 2017). When DSBs occur, DNA repair foci rapidly form at DSB sites, initiated by phosphorylation of the histone H2A variant H2AX at serine 139 (termed γ H2AX). γ H2AX enables the mobilization of DNA damage checkpoint proteins, which, in turn, facilitate the recruitment of DNA repair proteins at DSBs that enable DNA repair (Ciccio and Elledge, 2010). The DNA repair process drives the expression of cell cycle inhibitors such as cyclin-dependent kinase inhibitor 1, which inhibits the cell cycle upon DNA damage, allowing DNA repair and chromosomal integrity (Pérez-Yépez et al., 2018). In patients with idiopathic pulmonary fibrosis or in rodents with radiation, SiO₂ or bleomycin stimulation, DSBs play important roles in the epithelial–mesenchymal transition (EMT) during lung fibrosis (Duecker et al., 2018; Im et al., 2018; Naikawadi et al., 2016; Shifeng et al., 2019). This process may involve activating the mitosis-differentiation checkpoint (MDC), which is studied in tumors and may suppress potentially precancerous cells. However, the underlying mechanisms in silicosis are unclear. In keratinocytes and myoblasts, MDC activated by DSBs has been proposed to trigger terminal differentiation (Gandarillas et al., 2015; Puri et al., 2002). Based on these data, we hypothesize that SiO₂-induced DSBs and replication stress may directly promote the course of the EMT during silicosis, which might be treated by timely and effective DNA repair (Zeman and Cimprich, 2014).


DNA repair relies on microtubule (MT)-based trafficking of essential DNA repair proteins, including p53-binding protein 1 (53BP1, also known as TP53BP1), and the MT depolymerizer colchicine affects DNA repair by preventing DNA repair proteins from attaching to MTs for trafficking (Poruchynsky et al., 2015). Thus, stable MTs are required for this process. The acetylation of tubulin through α -tubulin N-acetyltransferase 1 (α -TAT1) facilitates the stability of MTs (Akella et al., 2010; Morley et al., 2016), and acetylated α -tubulin (Ac- α -Tub) serves as a marker for stable MTs. We previously reported that α -TAT1 and Ac- α -Tub levels decrease in silicotic nodules, and α -TAT1 overexpression inhibits myofibroblast differentiation induced by transforming growth factor beta 1, SiO₂ and angiotensin II (Shifeng et al., 2019; Xiaojun et al., 2016). Moreover, α -TAT1 silencing can induce accumulation of DNA damage, as well as promoting accumulation of HeLa cervical cancer cells and type II AECs in G2/M phase (Chien and Lin, 2016; Chien et al., 2016), which can initiate the EMT. As a result, α -TAT1 and Ac- α -Tub pathway-mediated MT stability may prevent the EMT by facilitating DNA repair, opening up a new avenue for anti-fibrosis therapy.

As mechanosensitive cytoskeleton components, α -TAT1 promotes the formation of Ac- α -Tub and efficient mechanosensation (Shida et al., 2010); Ac- α -Tub deacetylation occurs when the microenvironment stiffens, resulting in MT depolymerization (Hamant et al., 2019; Xu et al., 2017). Clinical

¹Basic Medicine College, North China University of Science and Technology, Tangshan 063210, China. ²Department of Neurosurgery, Tangshan People's Hospital, Tangshan 063210, China. ³School of Public Health, Medical Research Center, Hebei Key Laboratory for Organ Fibrosis Research, North China University of Science and Technology, Tangshan 063210, China. ⁴College of Traditional Chinese Medicine, North China University of Science and Technology, Tangshan 063210, China.

*These authors contributed equally to this work

†Author for correspondence (leimengpi@163.com)

 G.L., 0000-0002-3835-3122; S.C., 0000-0001-9540-6449; Y.Z., 0000-0002-8825-7884; H.X., 0000-0002-3655-3833; D.X., 0000-0001-5319-7546; Z.W., 0000-0002-4149-3847; X.G., 0000-0002-5905-2556; W.C., 0000-0001-9375-4378; N.M., 0000-0001-8947-3258; L.Z., 0000-0003-3216-3608; S.L., 0000-0001-8083-1071; S.L., 0000-0002-1910-5174

data have shown that in patients with interstitial lung disease, parenchymal shear stiffness is increased (Marinelli et al., 2017), and aggravation of the collagen (Col) I:ColIII ratio in the extracellular matrix (ECM) results in organ stiffening and fibrosis (Beam et al., 2015). We also previously found that dynamic changes in the ECM are crucial for the formation and progression of human coronary atherosclerosis (Yang et al., 1998) and human (coal) silicosis (Chen et al., 2008), and Ac- α -Tub deacetylation during silicosis may occur due to lung stiffening. Additionally, DNA repair proteins in cells cultured in a stiff matrix are prone to mislocalization (Xia et al., 2018). Thus, we hypothesized that matrix stiffness synergizes with SiO₂ to hamper the trafficking of essential DNA repair proteins via MT disruption, which triggers EMT during silicosis.

To explore this theory, we studied the effects of combining matrix stiffness and SiO₂ in a cell model, examined the EMT induced by replication stress, and further evaluated the effects of the α -TAT1 and Ac- α -Tub pathway on DNA repair.

RESULTS

DNA damage mainly affects epithelial cells in the lung tissue of silicotic rats

Upon prolonged SiO₂ inhalation, silicosis fibrosis was characterized by disorganized structure, multinodular confluent masses and diffused interstitial fibrosis (Fig. 1A, top panel). The expression level of γ H2AX, indicating DSBs (Albino et al., 2009), was upregulated within 16 weeks and then slightly decreased at week 24. The levels of 53BP1 and p21CIP1 (also known as CDKN1A) increased with time (Fig. 1D,E). The γ H2AX-positive cells were mainly located in the smaller nodules or around the larger nodules (Fig. 1A, bottom panel). Immunofluorescence (IF) revealed that γ H2AX fluorescence signals were stronger in the periphery of the silicotic nodules, which were co-positive for α -SMA (also known as ACTA2; fluorescence signal indicating myofibroblasts), but stronger α -SMA fluorescence was observed in the middle of the silicotic nodules without γ H2AX expression (Fig. 1B). Nevertheless, most surfactant protein D (SP-D, also known as SFTPD; fluorescence signal indicating AECs) and γ H2AX double-positive cells were located in the pulmonary alveolus and periphery of the silicotic nodules, suggesting DNA damage in the AECs (Fig. 1C). However, in addition to the apoptosis of AECs, there was also abnormal activation (Fig. S1C).

SiO₂-induced EMT is mediated by DNA damage and replication stress

Our previous studies have shown that the periphery of the silicotic nodules is an active region for DSBs and EMT in type II AECs (Shifeng et al., 2019). To investigate the DSBs during EMT of silicosis induced by SiO₂, we established an EMT model *in vitro* by SiO₂ exposure. The results showed that 0.1–10 μ g/cm² SiO₂ particles induced dose-dependent upregulation of γ H2AX in A549 cells (Fig. S2), and the increase of γ H2AX induced by 5 μ g/cm² SiO₂ peaked by 48 h (Fig. 2A,B). This induced the DNA-damage response (DDR), as previously reported, and elevation of cyclin-dependent kinase inhibitor 1 (p21CIP1) (initiated cell cycle arrest in the G1 phase) and 53BP1 adaptor (a protein activated later than γ H2AX that re-localizes to γ H2AX foci, leading to the formation of DNA repair foci) (Bártová et al., 2019) (Fig. 2A,B). In addition, SiO₂ caused an increased proportion of cells to undergo DNA synthesis (as shown by BrdU incorporation), indicating prolonged DNA replication (Fig. 2C). In keratinocytes, cell cycle deregulation and replication stress trigger squamous differentiation (Freije et al., 2014). Accordingly, immunohistochemistry (IHC)

images showed γ H2AX-positive cells exhibiting a large nucleus or binucleation after SiO₂ stimulation, which were positive for α -SMA staining (Fig. 2D). This phenomenon was also seen in mouse lung type II epithelial cells (MLE-12) and human embryonic lung fibroblasts (MRC-5) (Fig. 2E,F). In addition, a marked increase of myofibroblast markers α -SMA and Col I followed at 48 h (Fig. 2G). These results showed that SiO₂ caused DNA damage and replication stress prior to the EMT in A549 cells.

Matrix stiffness increases the ability of SiO₂ to induce DNA damage and the EMT

In silicosis patients, Col deposition in lung tissue leads to increased hardness of lung tissue (Marinelli et al., 2017), which is in part determined by the ratio of Col I:ColIII (Beam et al., 2015; Chen et al., 2008). The stiffness of ECM can affect the EMT (Barker et al., 2014) and DNA repair (Xia et al., 2018). We found that the ratio of Col I:ColIII increased continuously (Fig. S3B,C). In silicotic lesions with the EMT, as confirmed by α -SMA and vimentin upregulation and E-cadherin (also known as CDH1) downregulation (Fig. S3D,E), Col deposition was more severe than that in relatively normal alveoli of rats exposed to SiO₂ (Fig. S3A), indicating that the ECM stiffened upon EMT. To test whether SiO₂-stimulated ECM stiffening, but not Col itself, enhances EMT by causing DNA damage, we used matrix substrates with elastic moduli of 1 and 60 kPa covered with reconstituted basement membrane (rBM; commercially known as Matrigel) to represent normal and fibrotic valve tissue stiffness, respectively. Of note, under SiO₂ stimulation, AECs (A549 and MLE12) appeared shrunken on a 1 kPa matrix (soft matrix) and stretched on a 60 kPa matrix (stiff matrix) (Fig. 3A). In addition, SiO₂ stimulation promoted greater upregulation of the DNA damage markers (γ H2AX) and greater change of EMT markers (α -SMA and E-cadherin) in cells cultured on 60 kPa substrate than in cells cultured on 1 kPa substrate (Fig. 3B,C; Fig. S4), in accordance with a previous finding that rigid gels promote substrate-independent cell spreading and tension, with more α -SMA-positive stress fibers (Dingal et al., 2015). The changes were reversed by treatment with Y-27632 (a ROCK inhibitor), which inhibits myosin light chain phosphorylation and cell contractile force (Fig. 3B,C). In addition, the 60 kPa matrix resulted in higher and sustained γ H2AX and 53BP1 proteins in AEC cells after SiO₂ washout, indicating cells cultured on stiff matrix were more susceptible to SiO₂, and thus underwent the EMT (Fig. 3D–G; Fig. S4). These results suggest that the stiffness of matrix affects DNA damage repair, which may promote the EMT.

Matrix stiffness regulates mechanosensitive cytoskeleton Ac- α -Tub that affects the EMT

Ac- α -Tub is a mechanically sensitive cytoskeleton component that is downregulated under mechanical stimulation and is acetylated by α -TAT1 to maintain stability (Coombes et al., 2016). Similarly, we found that the levels of Ac- α -Tub and α -TAT1 in rat lung tissue were downregulated with increasing SiO₂ exposure time (Fig. 4A,B). The colocalization results for dual-channel IF images stained for Ac- α -Tub (green) and Col I (red, a harder ECM component that indicates stiffer matrix) showed that Ac- α -Tub intensity was weaker in silicotic nodules, with stronger Col I fluorescence signal in the silicosis 24-week group than in the control 24-week group (Fig. 4C). Cell viability and apoptosis were examined *in vitro* and *in vivo* to rule out the possibility that the expression of Ac- α -Tub was disrupted by contact inhibition or death. Although SiO₂ induced cell apoptosis and decrease in cellular activity (Fig. S1A,B), substrate stiffness was the main reason for the downregulation of Ac- α -Tub (Fig. 4F; Fig. S4). Next, we examined

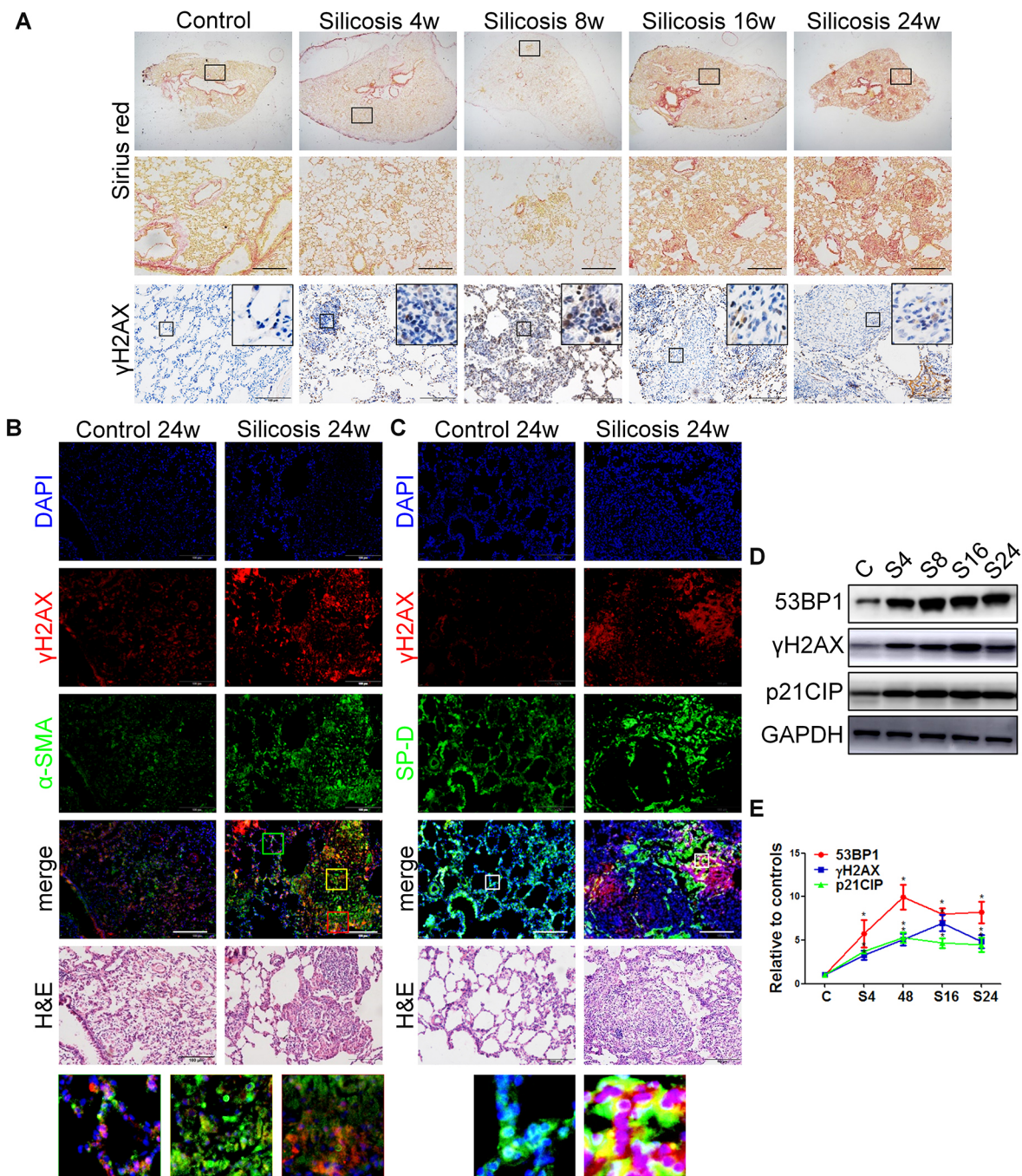


Fig. 1. DNA damage mainly affects epithelial cells in lung tissue of silicotic rats. (A) Sirius Red staining for lung morphology (top and middle panels) and IHC for γ H2AX (bottom panels) in the lung tissue of silicotic rats at 4, 8, 16 and 24 weeks of silicosis. Boxes indicate regions shown in higher magnification images (middle panels for Sirius Red images, insets for γ H2AX images). Scale bars: 100 μ m. (B) Colocalization of γ H2AX (red fluorescence indicating DNA damage) and α -SMA (green fluorescence indicating myofibroblasts) in a rat silicosis model. (C) Colocalization of γ H2AX (red fluorescence) and surfactant protein D (SP-D, green fluorescence indicating alveolar epithelial cells) in a rat silicosis model. Magenta fluorescence is the merged red and blue fluorescence signals, and yellow fluorescence is the merged red and green fluorescence signals, indicating colocalization. In B and C, DAPI staining shows nuclei and H&E staining reveals morphology. Boxes indicate regions shown at higher magnification below. Scale bars: 100 μ m. (D,E) Western blotting and corresponding densitometry data of γ H2AX, 53BP1 and p21CIP in rat lung tissue with SiO₂ exposure for 4, 8, 16 and 24 weeks (C, control; S, SiO₂ exposure). GAPDH is shown as a loading control. Data are presented as mean \pm s.d. $n=3$ per group. * $P<0.05$ (one-way ANOVA).

the involvement of Ac- α -Tub in SiO₂-induced and matrix stiffness-dependent EMT. We found that substrate stiffness inhibited Ac- α -Tub expression after SiO₂ washout, manifested as a significant decrease in Ac- α -Tub and α -TAT1 on 60 kPa matrix at 48 h compared with the levels at 0 h (Fig. 4D,E), whereas substrate stiffness promoted SiO₂-induced α -SMA expression (Fig. 4F; Fig. S4).

Acetylation of Ac- α -Tub by α -TAT1 attenuates SiO₂-induced DNA damage and DNA repair factor 53BP1 mislocalization

Based on reports that acetylation of α -tubulin facilitates enhanced interactions with and trafficking of cargos along MTs, and that the stability of MTs influences the intracellular trafficking of DNA repair proteins (Poruchynsky et al., 2015), we investigated

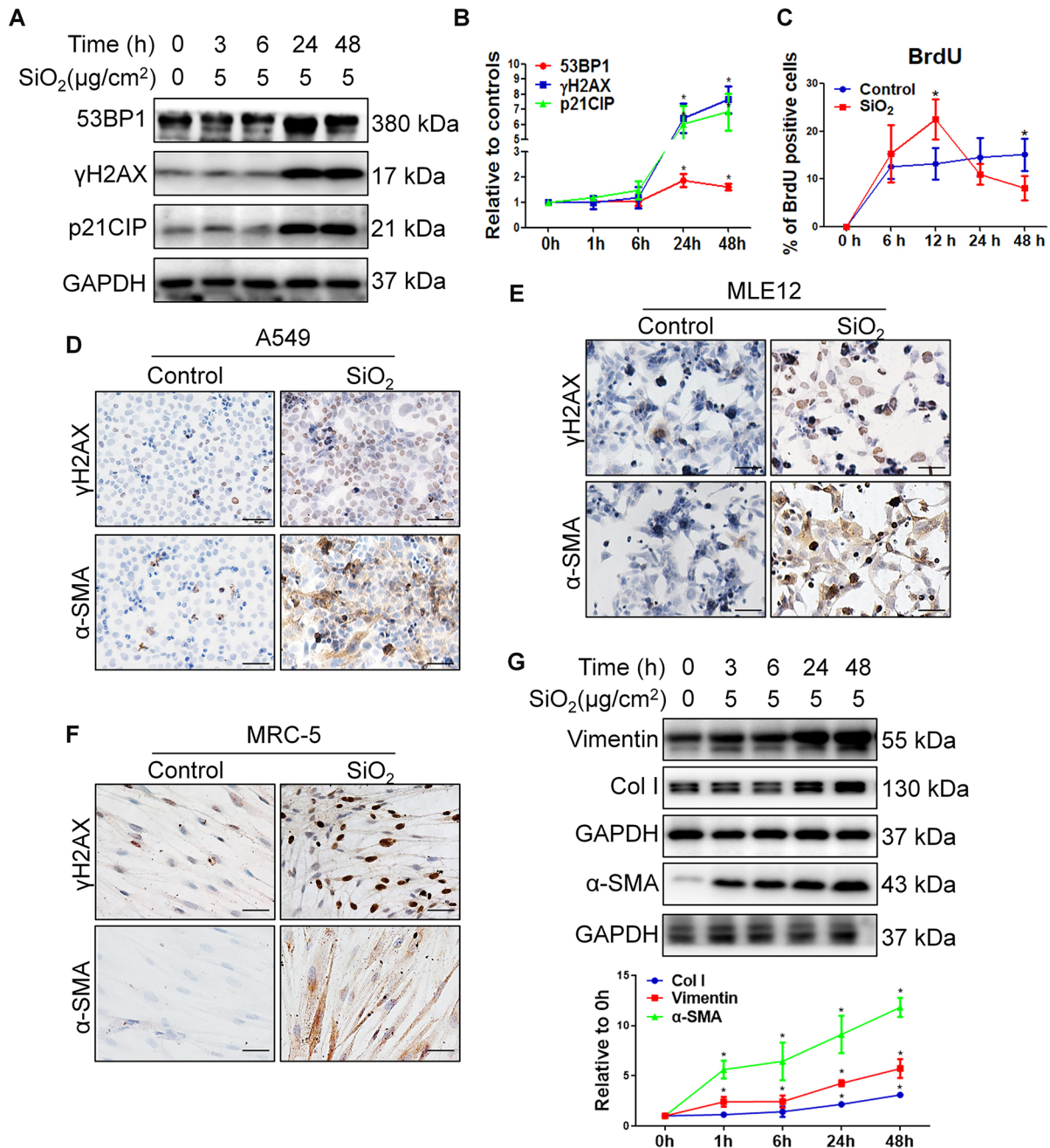


Fig. 2. DNA damage initiates the SiO₂-induced EMT of A549 cells. (A,B) Western blotting and corresponding densitometry data of γ H2AX, 53BP1 and p21CIP expression in A549 cells exposed to SiO₂ for the indicated times (0–48 h). GAPDH is shown as a loading control. (C) Flow cytometry quantitation of cells undergoing DNA synthesis (% BrdU positive). A549 cells were exposed to SiO₂ for the indicated times and are compared with controls with no SiO₂ treatment. (D–F) IHC for γ H2AX and α -SMA in (D) A549 cells, (E) MLE12 cells and (F) MRC-5 cells after exposure to SiO₂ for 48 h. Scale bars: 50 μ m. (G) Western blotting and corresponding densitometry data of vimentin, α -SMA and Col I expression in A549 cells exposed to SiO₂ for the indicated times (0–48 h). GAPDH is shown as a loading control. Data are presented as mean \pm s.d. $n=3$ per group. * $P<0.05$ (one-way ANOVA).

whether α -TAT1 plays a role in SiO₂-induced DNA damage and repair by regulating the acetylation of Ac- α -Tub. To this end, an *ATAT1*-pcDNA expression vector was used to overexpress α -TAT1 and increase downstream levels of Ac- α -Tub. Western blotting showed the effect of *ATAT1*-pcDNA overexpression (Fig. 5A). We also quantitated the level of γ H2AX in A549 cells pretreated with *ATAT1*-pcDNA and SiO₂. As shown in Fig. 5B, in empty vector (NC-pcDNA) control cells treated with SiO₂, the levels of γ H2AX remained high, with substantial amounts of γ H2AX still present at 24 and 48 h. However, in cells treated with

ATAT1-pcDNA, γ H2AX levels markedly decreased by 24 h and nearly disappeared at 48 h following SiO₂ washout. Immunostaining for γ H2AX together with the DNA repair factor 53BP1 was done to test 53BP1 mislocalization. Sudden mislocalization to the cytoplasm was frequently evident when stimulating with SiO₂ after NC-pcDNA transfection, whereas stable expression of α -TAT1 triggered a decrease in γ H2AX foci formation and relocalization of 53BP1 to these foci (Fig. 5C). As persistence of residual 53BP1 and γ H2AX foci is closely related to apoptosis and chromatin condensation (Markova et al., 2011), and mislocalization of DNA repair factor

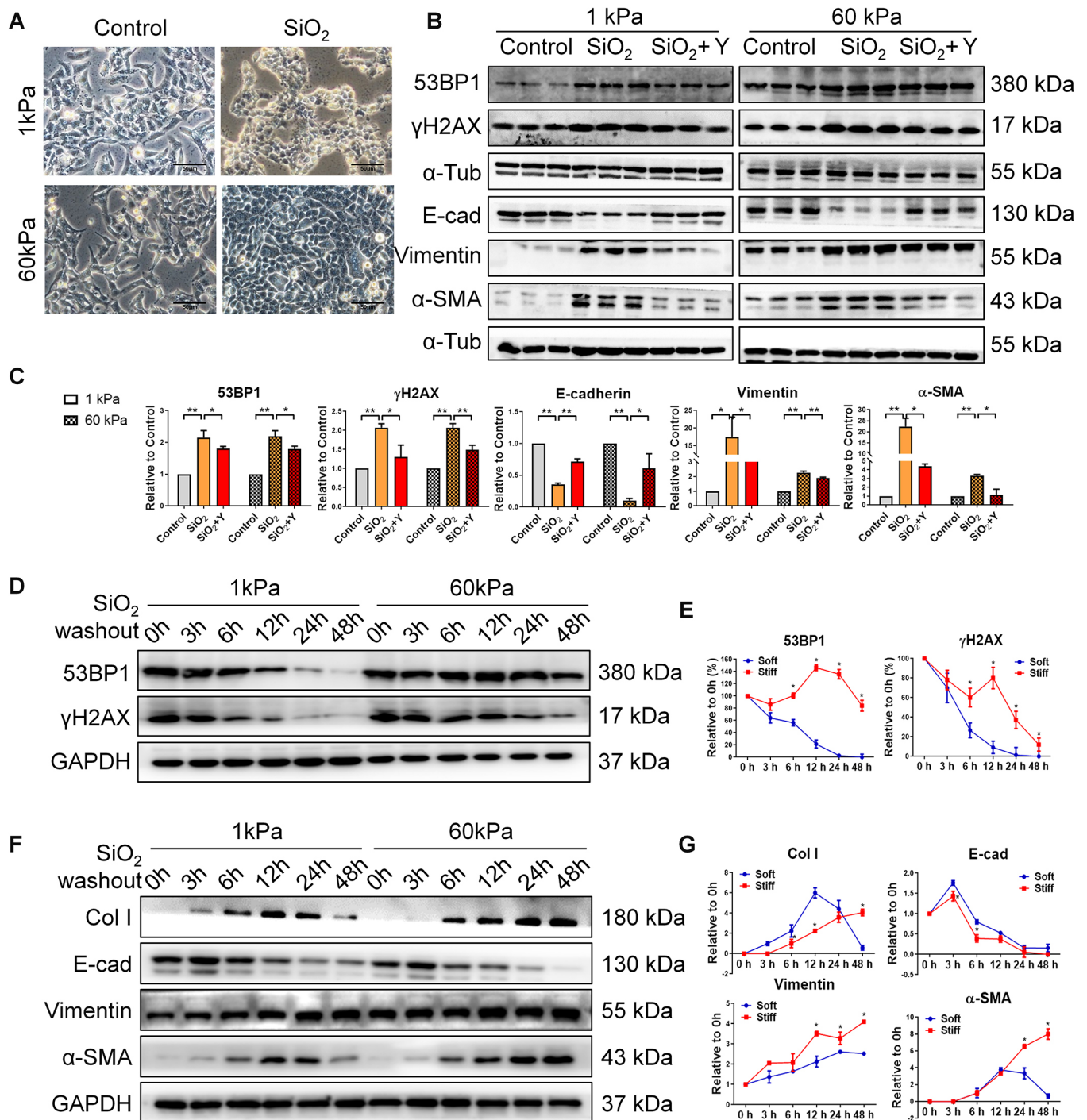


Fig. 3. Matrix stiffness increases the ability of SiO₂ to induce DNA damage and the EMT. (A) The morphology of A549 cells cultured on matrices (1 and 60 kPa) with or without SiO₂ for 48 h. Scale bars: 50 μm. (B, C) Western blotting and corresponding densitometry data of 53BP1, γH2AX, α-tubulin (α-Tub), E-cadherin (E-cad), vimentin and α-SMA expression in A549 cells cultured on matrices (1 and 60 kPa) with or without SiO₂ or Y-27632 (Y) for 48 h; the three lanes for each condition are biological replicates. (D–G) Western blotting and corresponding densitometry data of 53BP1, γH2AX, Col I, vimentin, α-SMA and E-cadherin expression in A549 cells cultured on matrices (1 kPa, soft; 60 kPa, stiff) after SiO₂ was washed out for the indicated times (0–48 h). GAPDH is shown as a loading control. Data are presented as mean±s.d. n=3 per group. *P<0.05 (one-way ANOVA).

delays DNA repair (Xia et al., 2018), our results indicated that α-TAT1 attenuated SiO₂-induced DNA damage through correlation with 53BP1 mislocalization.

53BP1 nuclear translocation depends on Ac-α-Tub

To further confirm whether Ac-α-Tub has the ability to guide the intracellular trafficking involved in DNA repair, we performed IF on

A549 cells fixed and incubated with anti-53BP1 and anti-Ac-α-Tub antibodies. 53BP1 exhibited cytoplasmic mislocalization within NC-pcDNA cells treated with SiO₂, whereas 53BP1 foci were distributed in the nucleus of A549 cells treated with ATAT1-pcDNA (Fig. 6A). Because MTs serve as orbitals for DNA repair protein transportation (Poruchynsky et al., 2015), we determined whether an antibody against the MT motor protein dynein could

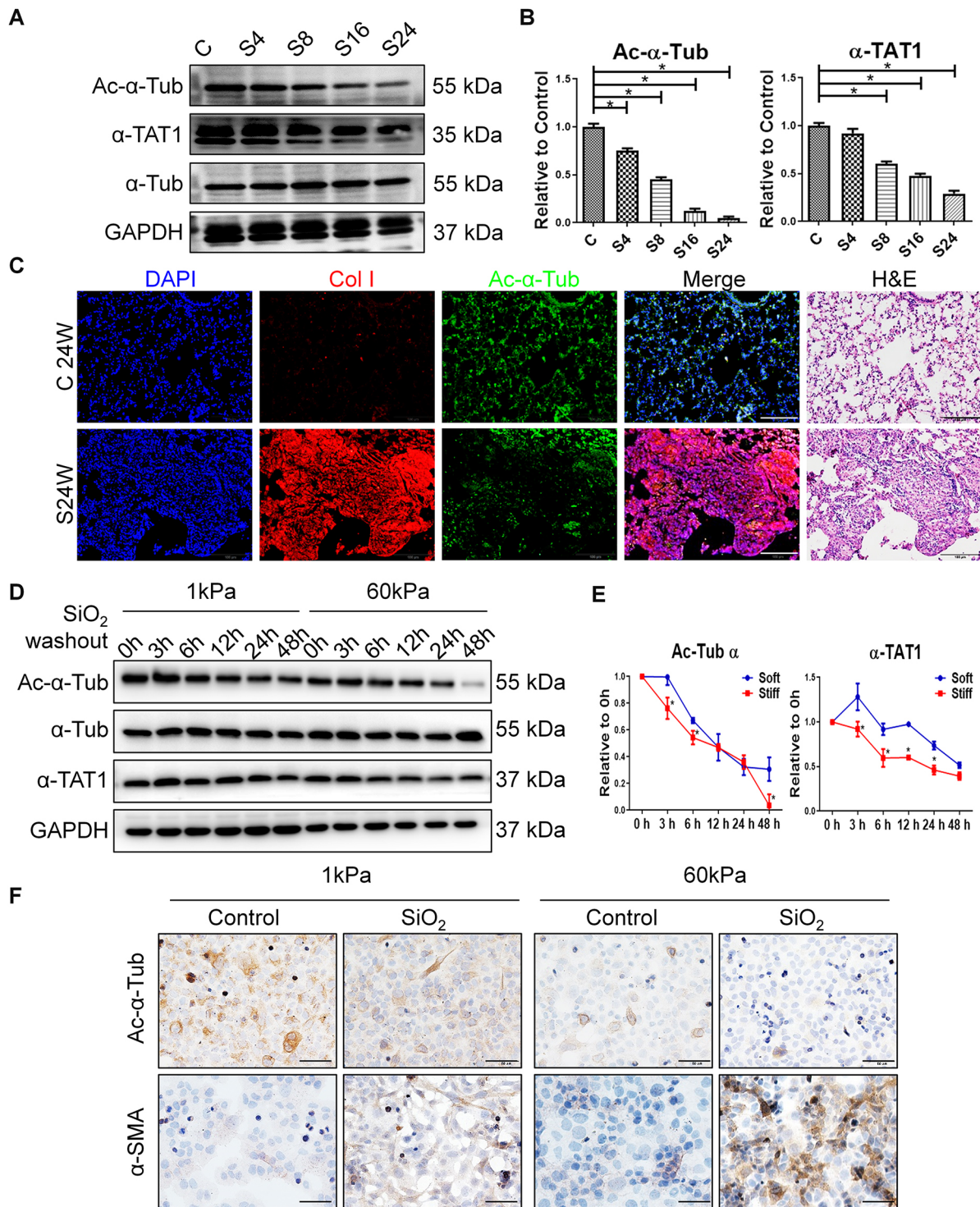


Fig. 4. Detection of Ac- α -Tub and α -TAT1 in silicotic rats and A549 cells induced by SiO₂ and matrix. (A,B) Western blotting and corresponding densitometry data of Ac- α -Tub and α -TAT1 expression in the lung tissue of control rats (C) and rats treated with SiO₂ for 4, 8, 16 and 24 weeks (S4, S8, S16 and S24, respectively). α -tubulin (α -Tub) and GAPDH blots are shown as controls. (C) IF of Col I and Ac- α -Tub co-expression in lung tissue of control (C24W) and SiO₂-treated (S24W) rats. DAPI staining shows nuclei, and H&E staining shows morphology. Scale bars: 100 μ m. (D,E) Western blotting and corresponding densitometry data of Ac- α -Tub and α -TAT1 expression in A549 cells cultured on matrices (1 kPa, soft; 60 kPa, stiff) after SiO₂ was washed out for the indicated times (0–48 h). α -Tub and GAPDH blots are shown as controls. (F) IHC of α -SMA and Ac- α -Tub in A549 cells. Scale bars: 50 μ m. Data in B and E are presented as mean \pm s.d. $n=3$ per group. * $P<0.05$ (one-way ANOVA).

co-immunoprecipitate (co-IP) 53BP1. We observed the co-IP of 53BP1 with dynein after treatment of A549 cells with *ATAT1*-pcDNA (Fig. 6B). This finding was consistent with experiments showing prominent fractionation of 53BP1 in the nucleus, where the

protein has functions, in *ATAT1*-pcDNA A549 cells (Fig. 6C). Conversely, we assessed the effects of MT disruption on SiO₂-induced DNA damage. A549 cells were incubated with 1 μ M colchicine for MT disruption or transfected with siRNA targeting

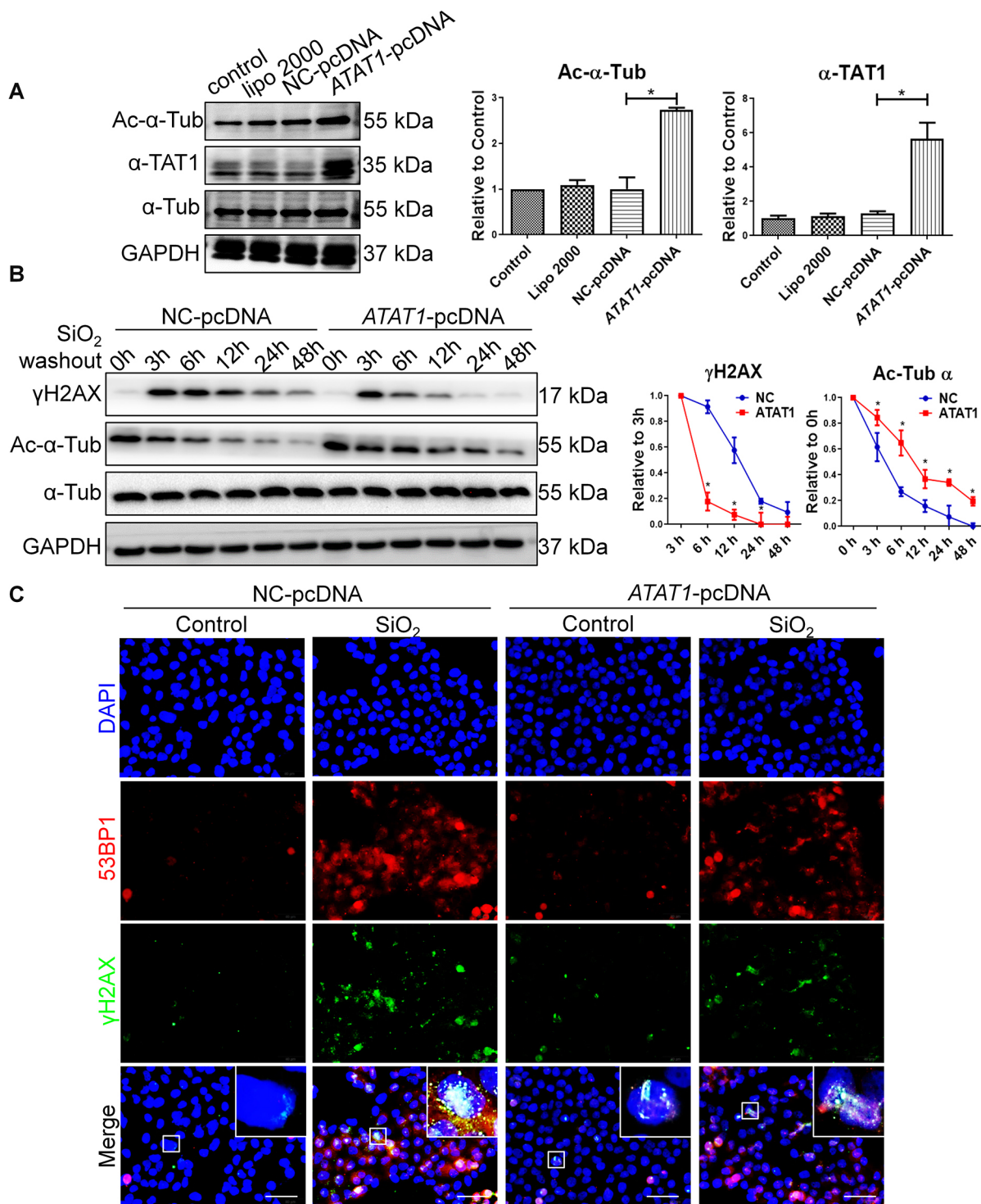


Fig. 5. Acetylation of Ac- α -Tub by α -TAT1 attenuates SiO₂-induced DNA damage and DNA repair factor 53BP1 mislocalization. (A) Effects of α -TAT1 overexpression (ATAT1-pcDNA) on α -TAT1 and Ac- α -Tub in A549 cells measured using western blotting (lipo 2000, mock transfection control; NC-pcDNA, empty vector control). (B) Western blotting and corresponding densitometry data of γ H2AX and Ac- α -Tub expression in A549 cells with ATAT1 overexpression and after SiO₂ was washed out for the indicated times (0–48 h). α -tubulin (α -Tub) and GAPDH blots are shown as loading controls. (C) IF imaging of 53BP1 and γ H2AX co-expression in A549 cells with or without α -TAT1 overexpression and SiO₂ treatment. Boxes indicate regions shown enlarged in inset images. Scale bars: 50 μ m. Data in A and B are presented as mean \pm s.d. $n=3$ per group. * $P<0.05$ (one-way ANOVA).

ATAT1 (ATAT1-siRNA; Fig. 7A) to reduce levels of α -TAT1 for 24 h, before SiO₂ stimulation for a further 24 h to monitor the levels of 53BP1 in the nucleus and cytoplasm. Ac- α -Tub was further inhibited by colchicine and ATAT1-siRNA treatments

compared with levels in control cells or cells treated with SiO₂ only (Fig. 7B). Disruption of Ac- α -Tub using colchicine and ATAT1-siRNA decreased the nucleus:cytoplasm ratio of 53BP1 localization (Fig. 7C). As previously demonstrated, the

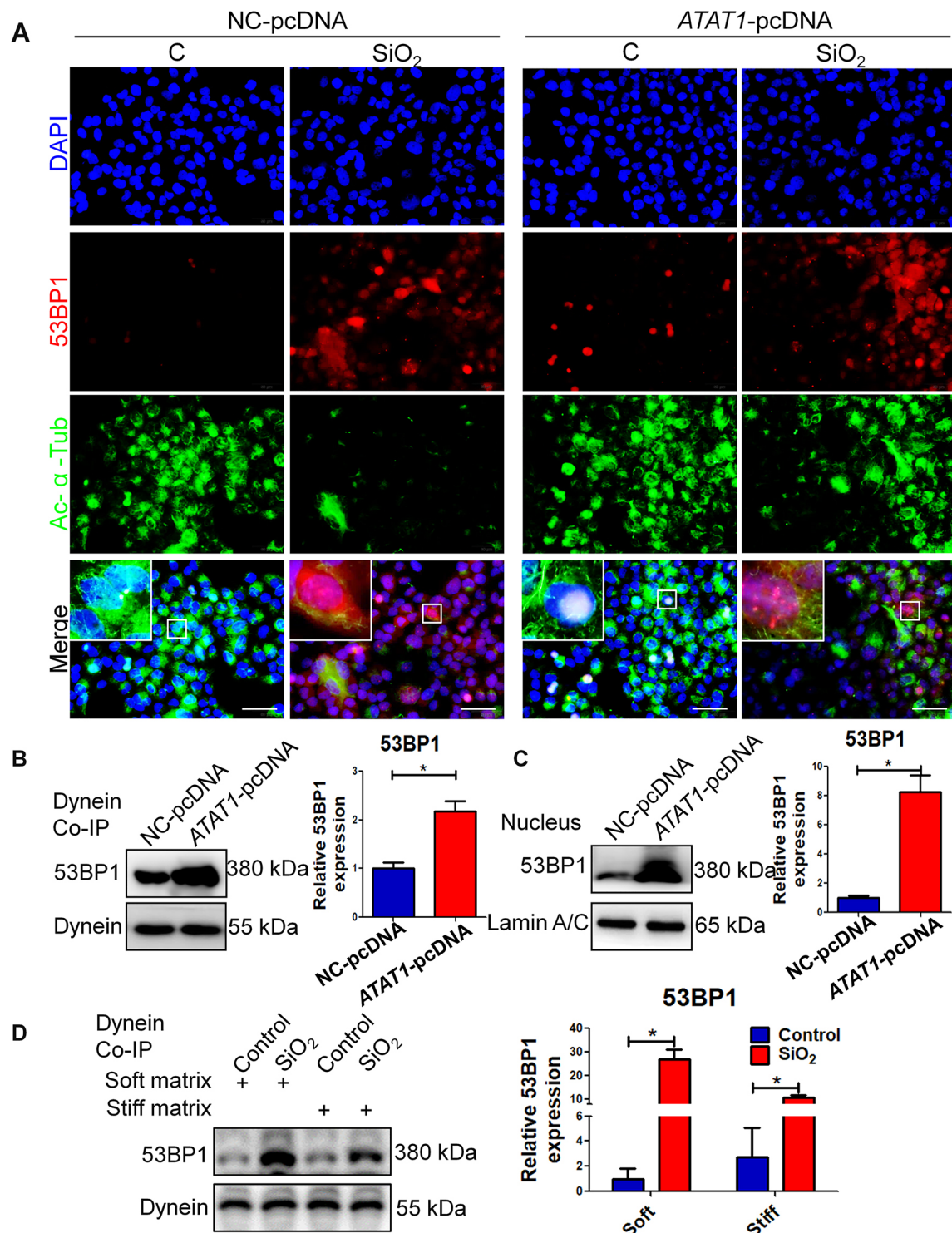


Fig. 6. Ac- α -Tub facilitates 53BP1 nuclear translocation. (A) IF images of 53BP1 and Ac- α -Tub co-expression in A549 cells (C, control). Boxes indicate regions shown enlarged in inset images. Scale bars: 50 μ m. (B) Binding of 53BP1 to dynein in A549 cells with or without ATAT1 overexpression was measured by co-IP. (C) The level of 53BP1 in nuclei of A549 cells was detected using western blotting. Lamin A/C blot is shown as a loading control for the nucleus. (D) Binding of 53BP1 to dynein in A549 cells with SiO₂ and matrix stimulation was measured by co-IP. Data are presented as mean \pm s.d. $n=3$ per group. * $P<0.05$ (t -test).

acetylation of Ac- α -Tub was influenced by the stiffness of the matrix. Thus, A549 cells were again cultured in soft and stiff matrix, followed by co-IP of 53BP1 with dynein. As expected, less 53BP1 could co-IP with dynein from cells cultured in stiff matrix compared with cells cultured in soft matrix (Fig. 6D),

supporting the idea that intracellular trafficking of 53BP1 may be susceptible to matrix stiffness. These results confirm the hypothesis that DDR proteins traffic to the nucleus on MTs, and that transport is stabilized by α -TAT1-mediated acetylation of Ac- α -Tub.

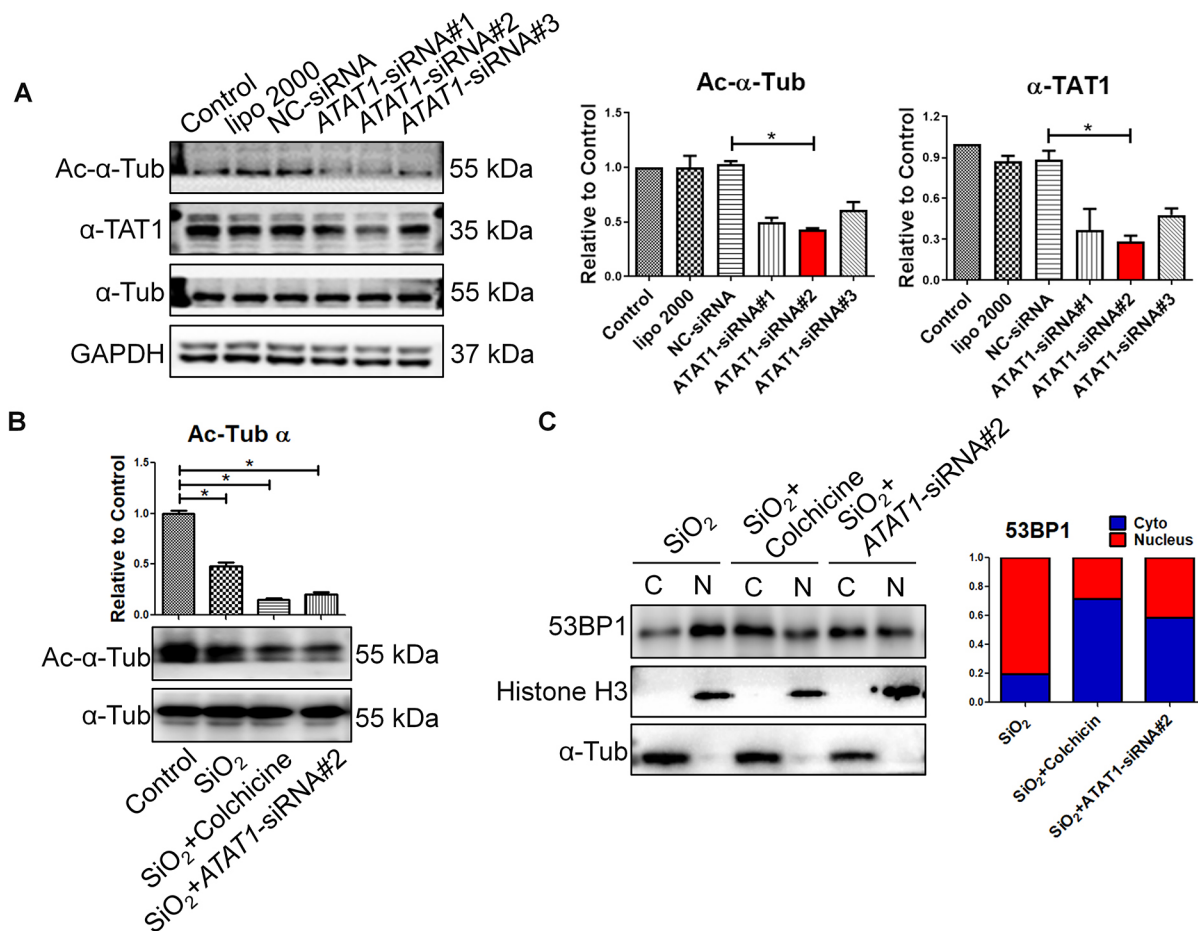


Fig. 7. 53BP1 nuclear translocation depends on Ac- α -Tub. (A) Effects of ATAT1-siRNAs on α -TAT1 and Ac- α -Tub expression in A549 cells, as measured using western blotting (lipo 2000, mock transfection control; NC-siRNA, negative control siRNA). α -tubulin (α -Tub) and GAPDH blots are shown as controls. (B) Western blotting and corresponding densitometry data of Ac- α -Tub expression in A549 cells treated with SiO₂, SiO₂ and colchicine, or SiO₂ and ATAT1-siRNA#2. α -Tub blot is shown as a loading control. (C) The 53BP1 in the nucleus (N) and cytoplasm (C) of A549 cells treated with SiO₂, SiO₂ and colchicine, or SiO₂ and ATAT1-siRNA#2 was detected using western blotting. Histone H3 and α -Tub blots are shown as loading controls for nuclear and cytoplasmic fractions, respectively. Data are presented as mean \pm s.d. $n=3$ per group. * $P<0.05$ (one-way ANOVA).

α -TAT1 overexpression attenuates replication stress and the EMT

Replication stress incurs mitosis failure that triggers MDC (Cho et al., 2019; Freije et al., 2014; Gandarillas and Freije, 2014). We explored whether α -TAT1 blocked replication stress and the EMT, thus explaining the potential beneficial effects of α -TAT1. A549 cells were transfected with ATAT1-pcDNA for 24 h before SiO₂ stimulation for an additional 24 h. Activation of α -TAT1 blocked the SiO₂-induced accumulation of cells in the S phase of the cell cycle (Fig. 8A,B; by flow cytometry). In addition, cells with high levels of α -TAT1 had reduced expression of the myofibroblast differentiation marker α -SMA (Fig. 8C), as well as a decrease in cell size and morphological crimples. The level of γ H2AX was also decreased upon ATAT1-pcDNA expression, and vimentin upregulation and E-cadherin downregulation were also observed in ATAT1-pcDNA cells (Fig. 8D,E).

DISCUSSION

Type II AECs are one of the main cells in lung tissue, which performs gas exchange function. They are continuously renewed and are exposed to mutagenic factors. Our study and others reported that DSBs mainly occur in type II AECs in both *in vivo* and *in vitro* models of silicosis, and are often accompanied by phenotypic

transformations including apoptosis, senescence and EMT (Shifeng et al., 2019). Studies of single-cell RNAseq from the lung tissue of bleomycin-treated mice have also found that, in addition to the apoptosis of AECs (including Type II AECs and Type I AECs), there is also abnormal activation of Type II AECs, which can play a role in injury repair and may be involved in the progression of fibrosis through abnormal activation of the EMT or other signal transduction pathways (Wu et al., 2020). Here, we showed that SiO₂ caused genetic damage of Type II AEC cells, which could be enhanced by matrix stiffness. This induced a DNA damage differentiation response, giving rise to phenotypic transformation (Fig. 8F). The concept of a 'differentiation checkpoint' has been proposed for decades (Gandarillas et al., 2015; Poleskaya and Rudnicki, 2002; Puri et al., 2002; Wang et al., 2014). In myogenic differentiation during embryonic development, the differentiation checkpoint is provoked by DNA damage and delays the global reprogramming of gene expression until the DNA is repaired, thereby guaranteeing genomic integrity to ensure the formation of normal differentiated cells. Moreover, the checkpoint-mediated inhibition of differentiation is reversible upon removal of stimulation (Puri et al., 2002). In silicosis, fibrotic stimulation persists and repeats, and DNA damage and DNA repair are ongoing (Xia et al., 2018). Our results found that cell proliferation and

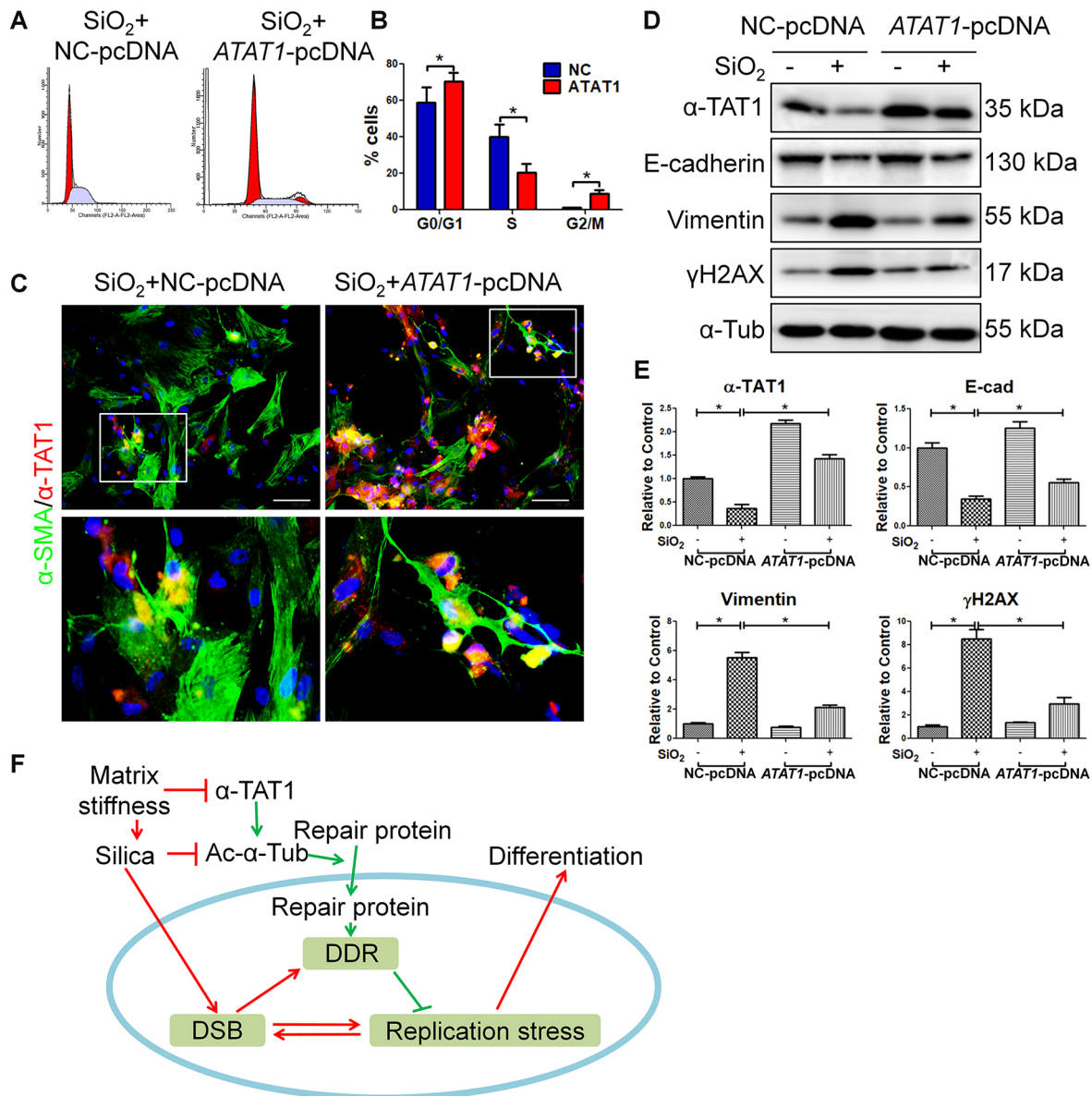


Fig. 8. α -TAT1 overexpression attenuates replication stress and EMT. (A,B) Cell cycle distribution of SiO₂-treated A549 cells with or without overexpression of α -TAT1 was measured using flow cytometry. (A) Representative flow cytometry cell cycle analysis of NC-pcDNA and ATAT1-pcDNA-transfected cells with concomitant SiO₂ stimulation. DNA content is represented on the x-axis, cell counts on the y-axis. (B) Quantification of A. Values on the y-axis represent percentage of cells at G0/G1, S and G2 phase. $n=3$ independent experiments. Results are mean \pm s.d. * $P<0.05$ (t -test) (C) IF images of α -SMA (green) and α -TAT1 (red) co-expression in SiO₂-treated A549 cells with or without overexpression of α -TAT1. Boxes indicate regions shown in enlarged images below. Scale bars: 50 μ m. (D,E) Western blotting and corresponding densitometry data of expression of α -TAT1, E-cadherin, vimentin, and γ H2AX in A549 cells treated with SiO₂ and ATAT1-pcDNA. α -tubulin (α -Tub) blot is shown as a loading control. Data are presented as mean \pm s.d. $n=3$ per group. * $P<0.05$ (one-way ANOVA). (F) The major processes underlying how matrix stiffness and SiO₂ synergize to regulate α -TAT1 and Ac- α -Tub, the DNA damage response and replication stress, which influences EMT. Red arrows indicate processes that promote fibrosis; green arrows indicate processes that inhibit fibrosis. For further explanation, see the Discussion section.

apoptosis coexisted in silicosis, and SiO₂ induced elevation of p21CIP1, leading to mitosis inhibition and persistence of residual 53BP1- γ H2AX foci (in relation to apoptosis and chromatin condensation; Markova et al., 2011). These results indicated that a significant portion of cells underwent replication stress, in accordance with a previous finding in epidermal keratinocytes (Freije et al., 2014; Sanz-Gómez et al., 2018). Interestingly, expression of the myofibroblast marker α -SMA was also enhanced in A549 cells. Therefore, DNA repair in terminally differentiated cells is biased towards the expressed genes through

transcription-coupled repair (Al-Khalaf et al., 2016; Lee et al., 2017). DNA damage does not halt differentiation once the program is established (Puri et al., 2002). This observation suggests that the phenotypic transformation of the EMT can happen as a result of sustained damage, which might initiate the differentiation checkpoint mechanism. Alveolar epithelial cells replaced by myofibroblasts result in lung remodeling and interfere with lung function (Shifeng et al., 2019).

Clinically, patients with silicosis are treated with alveolar lavage to reduce the concentration of SiO₂ in lung tissue (Kamel et al.,

1989); however, silicosis is still progressive. Even if most SiO₂ can be discharged, the toxicity of residual SiO₂ cannot be ruled out, and low doses of SiO₂ are liable to induce DNA damage (Zheng et al., 2017). We discovered that SiO₂ washout did not completely prevent EMT, especially for cells cultured on stiff substrate. This may be because the biological behavior of cells is due to their environment; in other words, the progression of fibrosis is also affected by the microenvironment *in situ*, including the increased stiffness of silicotic nodules (Marinelli et al., 2017), accumulation of fibrogenic cytokines, and adjacent cells (Yong et al., 2016). There is a link between substrate stiffness and cell spreading, which is related to cell survival and the EMT (Fu et al., 2010; Pelham and Wang, 1997; Yeung et al., 2005). Another study has highlighted that the regulation of cell function by matrix rigidity can be affected by other cell–matrix adhesion inputs, such as the ECM subtype. They found that matrix rigidity regulates a switch between TGF-β1-induced apoptosis and the EMT. Decreasing rigidity increases TGF-β1-induced apoptosis, which is more obvious when cells engage with fibronectin (FN) or the reconstituted basement membrane (rBM) compared with Col I. However, increasing rigidity results in the EMT, which is inhibited on compliant substrates independent of ECM subtypes, suggesting a central role for matrix mechanics in regulating the EMT (Leight et al., 2012). In addition to toxic or fibrogenic stimulation, mechanical injury has the independent function of promoting DNA damage (Xia et al., 2018). In addition, although it has been reported that substrate stiffness itself cannot modulate the EMT (Shukla et al., 2016), it has synergistic effects with particulate matter 2.5 on the phenotypic transformation of Type II AECs (Barker et al., 2014). We demonstrated that stiff matrix prolonged DNA damage. Cells may automatically eliminate cells with low genetic damage by means of differentiation (Sanz-Gómez et al., 2018). The damage differentiation response halts the cell cycle, which is mediated by 53BP1 (Fong et al., 2016; Lambrus et al., 2016). In our study, it was interesting to find that cells with polyploidy were mostly γH2AX- and α-SMA-positive. This model is supported by the fact that blocking mitosis causes DNA damage and ultimately triggers differentiation (Pilaz et al., 2016), although the molecules involved in the DNA damage differentiation response are currently unclear.

As mentioned above, DNA repair controls the time span of mitosis in the damage differentiation response. It is worth noting that acetylated tubulin represents the stable form of MTs in physiological conditions and can influence the trafficking of cargos (including DNA repair proteins) along MTs. Treating cells with nocodazole, which inhibits tubulin polymerization, or paclitaxel, which inhibits tubulin depolymerization, can enhance damage by DNA-damaging agents by prolonging DNA repair (Poruchynsky et al., 2015), which can directly trigger differentiation. In addition, cell mechanosensitivity is dependent upon the acetyltransferase activity of α-TAT1, which when absent, leads to a decrease in cellular elasticity (Morley et al., 2016). We previously revealed that quantitative promotion of microtubule acetylation may be a target for overcoming silicosis fibrosis (Xiaojun et al., 2016). In this study, α-TAT1 facilitated 53BP1 association with dynein and MTs via acetylating α-tubulin and stabilizing MTs. However, a previous study has revealed that α-TAT1 knockdown could directly block mitosis in HeLa and A549 cells independent of Ac-α-Tub (Chien et al., 2016). Another study showed that Ac-α-Tub is required for myofibroblast differentiation under soft substrate conditions (You et al., 2017). These results explain our findings that Ac-α-Tub levels can be maintained under soft substrate culture, but it is difficult to overcome SiO₂-induced EMT. Therefore, the differences in

the effects of Ac-α-Tub on cell fate decisions depend on variations in the microenvironment in which the cells are located, which affect the tubuloprotein (microtubule-associated proteins, MAP) transporters. Cell differentiation is the result of the crosstalk between microenvironment stimulation and signal activation. Clearly, the challenge of elucidating the mechanisms of how MTs and acetylation affect the development of silicosis, and establishing their clinical impact, still remain.

MATERIALS AND METHODS

Rat model

Animal studies were conducted using a protocol approved by the Institutional Animal Care and Use Committee of North China University of Science and Technology (No. 2013-038; Tangshan, China). Three-week-old male Sprague-Dawley rats with 180±10 g body weight were purchased from Vital River Laboratory Animal Technology Co. Ltd (SCXY 2009-0004; Beijing, China). They were fed and housed in a specific pathogen-free class laboratory at North China University of Science and Technology in accordance with the National Institutes of Health guidelines. A model of silicosis was made using the HOPE MED 8050 exposure control apparatus (HOPE Industry and Trade Co. Ltd., Tianjin, China), which is a non-invasive instrument for animal inhalation in a cabinet that sets a certain concentration of dust, according to a previously described protocol (Shifeng et al., 2019).

Cell culture and treatment

The human type II alveolar epithelial A549 cell line, mouse alveolar epithelial MLE12 cell line and human embryo lung fibroblast MRC-5 cell line were purchased from the Cell Bank of the Chinese Academy (Shanghai, China). Cells were treated with SiO₂ (1–10 μm in diameter, 0–10 μg/ml) (Zheng et al., 2017), matrix-coated plates and 1 μM colchicine (Wako Pure Chemical, Osaka, Japan) (Oyanagi et al., 2012) in serum-free medium (high glucose-DMEM medium, C11995500BT, GIBCO, USA). For overexpression vector (pcDNA) and siRNA transfection, cells were cultured in antibiotic-free medium.

Polyacrylamide gel preparation

The mechanical properties of the polyacrylamide gels were controlled by varying the percentage of acrylamide and bis-acrylamide as previously described (Leight et al., 2012), and elastic moduli of 1 kPa (3% acrylamide:0.1% bis-acrylamide) and 60 kPa (10% acrylamide:0.5% bis-acrylamide) were used in this study. Gels were covered with 140 μg/ml Matrigel for 2 h on ice. The gels were sterilized in 5% (v/v) isopropanol in phosphate-buffered saline (PBS) for 1 h at room temperature then rinsed two times with sterile PBS before plating with cells.

Plasmid transfection

Vectors encoding *Homo sapiens* α-tubulin acetyltransferase 1 (*ATAT1*) (NM_001031722.4) and cDNA clone (1230 base pairs) (TrueClone™ cDNA) were purchased from OriGene Technologies, Inc. (Rockville, MD, USA). Empty vector NC-pcDNA and ATAT1-pcDNA were transfected using Lipofectamine 2000 reagent (11668; Invitrogen, Carlsbad, CA, USA) according to the manufacturer's recommendations.

RNA interference of α-TAT1

Three sequences targeting human *ATAT1* were synthesized by Guangzhou Ruibo Biological Technology Co., Ltd. (Guangdong, China). Transfections were performed using Lipofectamine RNAiMAX (11668; Invitrogen). The three sequences were as follows: siRNA#1 sense, 5'-CGAGAACUCUU-CCAGUAUAdTdT-3'; siRNA#1 antisense, 5'-UAUACUGGAAGAGU-UCUCGdTdT-3'; siRNA#2 sense, 5'-GGCUCAUAAUGAGGUAGAA-dTdT-3'; siRNA#2 antisense, 5'-UUCUACCUCAUUAUGAGCCdTdT-3'; siRNA#3 sense, 5'-GAGCCAUUAUUGGUUUCAUdTdT-3'; siRNA#3 antisense, 5'-AUGAAACCAUAAUGGCUCdTdT-3'. siR-RuiboTM Negative control (NC-siRNA, siN0000001-1-10) was purchased from Ruibo Biological Technology Co., Ltd.

Histopathological examination

Lung tissues were fixed in 4% paraformaldehyde and later embedded in paraffin. Transverse sections of 4- μ m-thick slices were stained with Hematoxylin and Eosin (H&E) and Sirius Red (Maxin Company, Fuzhou, China). Images were acquired by microscopy under conventional light, and histopathological changes were observed under polarized light for Col analysis (BX53; Olympus, Tokyo, Japan). The histopathological images were only for pathological observation, and the pathological figures were reviewed by a clinical pathologist.

Immunohistochemistry and immunofluorescence

Immunohistochemistry (IHC) and immunofluorescence (IF) were performed as previously reported (Shifeng et al., 2019). Cells were cultured at a density of 6×10^3 cells/well in a four-well chamber slide for 12 h to 50% confluency, and then were treated as described above. Paraffin sections of the lung tissue and cell slides were incubated with antibodies against α -smooth muscle actin (α -SMA; 1:200; 1184-1; Epitomics, Burlingame, CA, USA), collagen type I (Col I; 1:200; ab34710; Abcam, Cambridge, MA, USA), α -TAT1 (1:100; ab58742; Abcam), 53BP1 (1:150; GTX64370; GeneTex, Inc., Irvine, CA, USA), γ H2AX (1:150; GTX628789; GeneTex, Inc.) and Ac- α -Tub (1:200; sc-23950; Santa Cruz Biotechnology, Santa Cruz, CA, USA). After that, sections were incubated with products from Novex (Life Technologies, Frederick, MD): donkey anti-rabbit IgG (H+L) FITC (A16024), donkey anti-mouse IgG (H+L) TRITC (A16016) mixture or donkey anti-rabbit IgG (H+L) TRITC (A16028) and donkey anti-mouse IgG (H+L) FITC (A16018) mixture for 60 min each at 37°C in blocking buffer. The slides were then counterstained with DAPI (5 mg/ml; Beyotime, Haimen, China) and visualized using an Olympus DP80 microscope (Olympus Soft Imaging). Finally, slides of lung tissue were re-stained with H&E to verify the histomorphology.

Western blot analysis

Western blotting was performed as previously described (Shifeng et al., 2019). The primary antibodies used were those against Col I (1:2000; ab34710; Abcam), p21CIP1 (1:1500; ab109520; Abcam), α -TAT1 (1:3000; ab58742; Abcam), dynein (1:3000; ab23905; Abcam), α -SMA (1:3000; 1184-1; Epitomics), FN (1:2000; ab45688; Epitomics), vimentin (1:3000; AF7013; Affinity Biosciences, Cincinnati, OH, USA), Col III (1:2000; GTX101043; GeneTex, Inc.), 53BP1 (1:2000; GTX64370; GeneTex, Inc.), γ H2AX (1:3000; GTX628789; GeneTex, Inc.), E-cadherin (1:3000; GTX100443; GeneTex, Inc.), histone H3 (1:4000; GTX 122148; GeneTex, Inc.), Ac- α -Tub (1:3000; sc-23950; Santa Cruz Biotechnology) and GAPDH (1:5000; sc-25778; Santa Cruz Biotechnology). The results were normalized to the loading control and expressed as the fold of the specific bands to the control group. Western blotting was repeated at least three times.

Flow cytometry analysis

For cell-cycle analysis, A549 cells (1×10^6) were collected and fixed in ice-cold 70% alcohol. After washing with cold PBS, resuspending and treating with RNaseA (50 μ g/ml, Beyotime, Jiangsu, China), cells were stained with propidium iodide (PI; BD Biosciences, Franklin Lakes, NJ, USA) in the dark for 30 min. A total of 20,000 events were gated and acquired in list mode for every sample. The cell cycle distribution was collected using a flow cytometer (FACS Calibur; BD Biosciences) and analyzed by BD Cell Quest Pro software. For DNA synthesis analyses, cells were incubated with 10 μ M bromodeoxyuridine (BrdU; Sigma-Aldrich) for 1.5 h, and then fixed, permeabilized and treated with DNase. Then cells were labeled with anti-BrdU antibody (ab8152; Abcam) followed by goat anti-mouse FITC-conjugated antibody (ab6785; Abcam), according to the manufacturer's protocol. PI was added and cells were analyzed by flow cytometry.

Co-immunoprecipitation

The interaction of dynein with 53BP1 was evaluated by co-immunoprecipitation (co-IP) (Li et al., 2020). The cells were lysed in RIPA buffer (R0020; Solarbio Life Science, Beijing, China) containing 1% protease inhibitors (04693132001, Roche). Then 30 μ l of sepharose beads (FO115; Santa Cruz Biotechnology) and cell lysates (2 mg/ml) were mixed

to a volume of 400 μ l and incubated for 2 h at 4°C on a shaker for pre-clearing. The cleared supernatant was incubated overnight with anti-dynein (ab249262, Abcam) and Protein A sepharose overnight at 4°C. The beads were collected and washed three times with PBS before being boiled in 2 \times loading buffer at 95°C for 5 min. Western blotting was used to analyze the co-IP results.

Terminal deoxynucleotidyl transferase dUTP nick end labeling assay

The presence of apoptotic cells was evaluated by the terminal deoxynucleotidyl transferase dUTP nick end labeling (TUNEL) assay according to the manufacturer's instructions (S7110, Merck). Percent apoptosis was determined by counting the number of apoptotic cells and dividing by the total number of cells in the field (five high-power fields per slide).

Cell counting kit-8

Cells (10^4 cells per well and three wells per group) were seeded in 96-well plates. Quantitative cell viability was evaluated according to the manufacturer's protocol for the Cell Counting Kit-8 (CCK8) assay (ZP328, ZOMANBIO). The optical density (OD) was read at 450 nm to obtain a cell growth curve.

Statistical analyses

Data were analyzed using SPSS 22.0. All results are expressed as the mean \pm s.d. For comparisons between two conditions, we used the *t*-test. For multiple comparisons between conditions, a one-way ANOVA was used. For post hoc testing, the least significant difference test was used when the variance was constant, and the Tamhane's test was used when there was heterogeneity of variance. $P < 0.05$ was considered statistically significant.

Competing interests

The authors declare no competing or financial interests.

Author contributions

Conceptualization: H.X., Shifeng Li; Methodology: G.L., S.C., Y.Z.; Software: S.C., L.Z.; Validation: G.L., S.C., Y.Z., X.G., W.C.; Formal analysis: D.X., Z.W.; Investigation: G.L., S.C., N.M., Shumin Li; Resources: Shifeng Li; Writing - original draft: G.L., S.C.; Writing - review & editing: H.X., Shifeng Li; Supervision: F.Y., H.L., Shifeng Li; Project administration: Shifeng Li; Funding acquisition: H.X., Z.W., F.Y., Shifeng Li.

Funding

This work was supported by the National Natural Science Foundation of China (82003406, 81972988), the Natural Science Foundation of Hebei Province (H2020209287), the Colleges and Universities in Hebei Province Science and Technology Research Project (ZD2019077), the Science and Technology Plan Project of Tangshan City (20130206b) and the Medical Research Foundation of Hebei Health Commission (20191107).

Supplementary information

Supplementary information available online at <https://jcs.biologists.org/lookup/doi/10.1242/jcs.243394.supplemental>

Peer review history

The peer review history is available online at <https://jcs.biologists.org/lookup/doi/10.1242/jcs.243394.reviewer-comments.pdf>

References

- Akella, J. S., Wloga, D., Kim, J., Starostina, N. G., Lyons-Abbott, S., Morrisette, N. S., Dougan, S. T., Kipreos, E. T. and Gaertig, J. (2010). MEC-17 is an alpha-tubulin acetyltransferase. *Nature* **467**, 218-222. doi:10.1038/nature09324
- Al-Khalaf, M. H., Blake, L. E., Larsen, B. D., Bell, R. A., Brunette, S., Parks, R. J., Rudnicki, M. A., McKinnon, P. J., Jeffrey Dilworth, F. and Megeney, L. A. (2016). Temporal activation of XRCC1-mediated DNA repair is essential for muscle differentiation. *Cell Discov.* **2**, 15041. doi:10.1038/celldisc.2015.41
- Albino, A. P., Jorgensen, E. D., Rainey, P., Gillman, G., Clark, T. J., Gietl, D., Zhao, H., Traganos, F. and Darzynkiewicz, Z. (2009). gammaH2AX: a potential DNA damage response biomarker for assessing toxicological risk of tobacco products. *Mutat. Res.* **678**, 43-52. doi:10.1016/j.mrgentox.2009.06.009
- Barker, T. H., Dysart, M. M., Brown, A. C., Douglas, A. M., Fiore, V. F., Russell, A. G. and Committee, H. E. I. H. R. (2014). Synergistic effects of particulate

- matter and substrate stiffness on epithelial-to-mesenchymal transition. *Res. Rep. Health Eff. Inst.* **182**, 3–41.
- Bártová, E., Legartová, S., Dundr, M. and Suchánková, J.** (2019). A role of the 53BP1 protein in genome protection: structural and functional characteristics of 53BP1-dependent DNA repair. *Aging (Albany NY)* **11**, 2488–2511. doi:10.18632/aging.101917
- Beam, J., Botta, A., Ye, J., Soliman, H., Matier, B. J., Forrest, M., MacLeod, K. M. and Ghosh, S.** (2015). Excess linoleic acid increases collagen I/III ratio and “Stiffens” the heart muscle following high fat diets. *J. Biol. Chem.* **290**, 23371–23384. doi:10.1074/jbc.M115.682195
- Chen, P., Yang, F., Yan, J. B., Li, Q., Zhang, L. J., Wang, R. M., Li, D. D. and Wu, K. F.** (2008). [Antifibrotic effect of N-acetyl-seryl-aspartyl-lysyl-proline mediated by the regulation of collagen synthesis and degradation in lungs of rats with silicosis]. *China Occupational Med.* **35**, 274–277.
- Chien, J. Y. and Lin, C. H.** (2016). alphaTAT1: a potential therapeutic target in cancer? *Cell Death Dis.* **7**, e2172. doi:10.1038/cddis.2016.46
- Chien, J. Y., Tsen, S. D., Chien, C. C., Liu, H. W., Tung, C. Y. and Lin, C. H.** (2016). alphaTAT1 downregulation induces mitotic catastrophe in HeLa and A549 cells. *Cell Death Discov.* **2**, 16006. doi:10.1038/cddiscovery.2016.6
- Cho, S., Vashisth, M., Abbas, A., Majkut, S., Vogel, K., Xia, Y., Ivanovska, I. L., Irianto, J., Tewari, M., Zhu, K. et al.** (2019). Mechanosensing by the lamina protects against nuclear rupture, DNA damage, and cell-cycle arrest. *Dev. Cell* **49**, 920–935.e5. doi:10.1016/j.devcel.2019.04.020
- Ciccio, A. and Elledge, S. J.** (2010). The DNA damage response: making it safe to play with knives. *Mol. Cell* **40**, 179–204. doi:10.1016/j.molcel.2010.09.019
- Cohen, R. A., Petsonk, E. L., Rose, C., Young, B., Regier, M., Najmuddin, A., Abraham, J. L., Churg, A. and Green, F. H.** (2016). Lung pathology in U.S. Coal workers with rapidly progressive pneumoconiosis implicates silica and silicates. *Am. J. Respir. Crit. Care Med.* **193**, 673–680. doi:10.1164/rccm.201505-1014OC
- Coombes, C., Yamamoto, A., McClellan, M., Reid, T. A., Plooster, M., Luxton, G. W., Alper, J., Howard, J. and Gardner, M. K.** (2016). Mechanism of microtubule lumen entry for the alpha-tubulin acetyltransferase enzyme alphaTAT1. *Proc. Natl. Acad. Sci. USA* **113**, E7176–E7184. doi:10.1073/pnas.1605397113
- Dingal, P. C. D. P., Bradshaw, A. M., Cho, S., Raab, M., Buxboim, A., Swift, J. and Discher, D. E.** (2015). Fractal heterogeneity in minimal matrix models of scars modulates stiff-niche stem-cell responses via nuclear exit of a mechanorepressor. *Nat. Mater.* **14**, 951–960. doi:10.1038/nmat4350
- Duecker, R., Baer, P., Eickmeier, O., Strecker, M., Kurz, J., Schaible, A., Henrich, D., Zielen, S. and Schubert, R.** (2018). Oxidative stress-driven pulmonary inflammation and fibrosis in a mouse model of human ataxia-telangiectasia. *Redox Biol.* **14**, 645–655. doi:10.1016/j.redox.2017.11.006
- Fong, C. S., Mazo, G., Das, T., Goodman, J., Kim, M., O'Rourke, B. P., Izquierdo, D. and Tsou, M. F.** (2016). 53BP1 and USP28 mediate p53-dependent cell cycle arrest in response to centrosome loss and prolonged mitosis. *Elife* **5**, e16270. doi:10.7554/eLife.16270
- Freije, A., Molinuevo, R., Ceballos, L., Cagigas, M., Alonso-Lecue, P., Rodriguez, R., Menendez, P., Aberdam, D., De Diego, E. and Gandarillas, A.** (2014). Inactivation of p53 in human keratinocytes leads to squamous differentiation and shedding via replication stress and mitotic slippage. *Cell Rep* **9**, 1349–1360. doi:10.1016/j.celrep.2014.10.012
- Fu, J., Wang, Y.-K., Yang, M. T., Desai, R. A., Yu, X., Liu, Z. and Chen, C. S.** (2010). Mechanical regulation of cell function with geometrically modulated elastomeric substrates. *Nat. Methods* **7**, 733–736. doi:10.1038/nmeth.1487
- Gandarillas, A. and Freije, A.** (2014). Cycling up the epidermis: reconciling 100 years of debate. *Exp. Dermatol.* **23**, 87–91. doi:10.1111/exd.12287
- Gandarillas, A., Molinuevo, R., Freije, A. and Alonso-Lecue, P.** (2015). The mitosis-differentiation checkpoint, another guardian of the epidermal genome. *Mol. Cell Oncol.* **2**, e997127. doi:10.1080/23723556.2014.997127
- Hamant, O., Inoue, D., Bouchez, D., Dumais, J. and Mjolsness, E.** (2019). Are microtubules tension sensors? *Nat. Commun.* **10**, 2360. doi:10.1038/s41467-019-10207-y
- Im, J., Lawrence, J., Seelig, D. and Nho, R. S.** (2018). FoxM1-dependent RAD51 and BRCA2 signaling protects idiopathic pulmonary fibrosis fibroblasts from radiation-induced cell death. *Cell Death Dis.* **9**, 584. doi:10.1038/s41419-018-0652-4
- Kamel, A., Hamzaoui, A., Hamzaoui, K., Zaimi, M., Jeguirim, M. S., Chabbou, A. and el Charbi, B.** (1989). [Alveolar lavage in silicosis]. *Tunis. Med.* **67**, 311–314.
- Lambrus, B. G., Daggubati, V., Uetake, Y., Scott, P. M., Clutario, K. M., Sluder, G. and Holland, A. J.** (2016). A USP28-53BP1-p53-p21 signaling axis arrests growth after centrosome loss or prolonged mitosis. *J. Cell Biol.* **214**, 143–153. doi:10.1083/jcb.201604054
- Lee, J.-H., Park, S.-J., Kim, S. W., Hariharasudhan, G., Jung, S.-M., Jun, S., Yong, J. and Jin You, H.** (2017). c-Fos-dependent miR-22 targets MDC1 and regulates DNA repair in terminally differentiated cells. *Oncotarget* **8**, 48204–48221. doi:10.18632/oncotarget.18389
- Leight, J. L., Wozniak, M. A., Chen, S., Lynch, M.-L. and Chen, C. S.** (2012). Matrix rigidity regulates a switch between TGF-beta1-induced apoptosis and epithelial-mesenchymal transition. *Mol. Biol. Cell* **23**, 781–791. doi:10.1091/mbc.e11-06-0537
- Li, S., Wei, Z., Li, G., Zhang, Q., Niu, S., Xu, D., Mao, N., Chen, S., Gao, X., Cai, W. et al.** (2020). Silica perturbs primary cilia and causes myofibroblast differentiation during silicosis by reduction of the KIF3A-repressor GLI3 complex. *Theranostics* **10**, 1719–1732. doi:10.7150/tno.37049
- Marinelli, J. P., Levin, D. L., Vassallo, R., Carter, R. E., Hubmayr, R. D., Ehman, R. L. and McGee, K. P.** (2017). Quantitative assessment of lung stiffness in patients with interstitial lung disease using MR elastography. *J. Magn. Reson. Imaging* **46**, 365–374. doi:10.1002/jmri.25579
- Markova, E., Torudd, J. and Belyaev, I.** (2011). Long time persistence of residual 53BP1/gamma-H2AX foci in human lymphocytes in relationship to apoptosis, chromatin condensation and biological dosimetry. *Int. J. Radiat. Biol.* **87**, 736–745. doi:10.3109/09553002.2011.577504
- Morley, S. J., Qi, Y., Iovino, L., Andolfi, L., Guo, D., Kalebic, N., Castaldi, L., Tischer, C., Portulano, C., Bolasco, G. et al.** (2016). Acetylated tubulin is essential for touch sensation in mice. *Elife* **5**, e20813. doi:10.7554/eLife.20813
- Naikwadi, R. P., Disayabutr, S., Mallavia, B., Donne, M. L., Green, G., La, J. L., Rock, J. R., Looney, M. R. and Wolters, P. J.** (2016). Telomere dysfunction in alveolar epithelial cells causes lung remodeling and fibrosis. *JCI Insight* **1**, e86704. doi:10.1172/jci.insight.86704
- Oyanagi, J., Ogawa, T., Sato, H., Higashi, S. and Miyazaki, K.** (2012). Epithelial-mesenchymal transition stimulates human cancer cells to extend microtubule-based invasive protrusions and suppresses cell growth in collagen gel. *PLoS ONE* **7**, e53209. doi:10.1371/journal.pone.0053209
- Pelham, R. J., Jr. and Wang, Y.** (1997). Cell locomotion and focal adhesions are regulated by substrate flexibility. *Proc. Natl. Acad. Sci. U.S.A.* **94**, 13661–13665. doi:10.1073/pnas.94.25.13661
- Pérez-Yépez, E. A., Saldívar-Ceron, H. I., Villamar-Cruz, O., Perez-Plasencia, C. and Arias-Romero, L. E.** (2018). Corrigendum to “p21 Activated kinase 1: Nuclear activity and its role during DNA damage repair” [DNA Repair 65 (2018) 42–46]. *DNA Repair (Amst)* **72**, 115. doi:10.1016/j.dnarep.2018.08.001
- Pilaz, L. J., McMahon, J. J., Miller, E. E., Lennox, A. L., Suzuki, A., Salmon, E. and Silver, D. L.** (2016). Prolonged mitosis of neural progenitors alters cell fate in the developing brain. *Neuron* **89**, 83–99. doi:10.1016/j.neuron.2015.12.007
- Poleskaya, A. and Rudnicki, M. A.** (2002). A MyoD-dependent differentiation checkpoint: ensuring genome integrity. *Dev. Cell* **3**, 757–758. doi:10.1016/S1534-5807(02)00372-6
- Poruchynsky, M. S., Komlodi-Pasztor, E., Trostel, S., Wilkerson, J., Regairaz, M., Pommier, Y., Zhang, X., Kumar Maity, T., Robey, R., Burotto, M. et al.** (2015). Microtubule-targeting agents augment the toxicity of DNA-damaging agents by disrupting intracellular trafficking of DNA repair proteins. *Proc. Natl. Acad. Sci. USA* **112**, 1571–1576. doi:10.1073/pnas.1416418112
- Puri, P. L., Bhakta, K., Wood, L. D., Costanzo, A., Zhu, J. and Wang, J. Y. J.** (2002). A myogenic differentiation checkpoint activated by genotoxic stress. *Nat. Genet.* **32**, 585–593. doi:10.1038/ng1023
- Sanz-Gómez, N., Freije, A., Ceballos, L., Obeso, S., Sanz, J. R., García-Reija, F., Morales-Angulo, C. and Gandarillas, A.** (2018). Response of head and neck epithelial cells to a DNA damage-differentiation checkpoint involving polyploidization. *Head Neck* **40**, 2487–2497. doi:10.1002/hed.25376
- Shida, T., Cueva, J. G., Xu, Z., Goodman, M. B. and Nachury, M. V.** (2010). The major alpha-tubulin K40 acetyltransferase alphaTAT1 promotes rapid ciliogenesis and efficient mechanosensation. *Proc. Natl. Acad. Sci. USA* **107**, 21517–21522. doi:10.1073/pnas.1013728107
- Shifeng, L., Hong, X., Xue, Y., Siyu, N., Qiaodan, Z., Dingjie, X., Lijuan, Z., Zhongqiu, W., Xuemin, G., Wenchen, C. et al.** (2019). Ac-SDKP increases alpha-TAT 1 and promotes the apoptosis in lung fibroblasts and epithelial cells double-stimulated with TGF-beta1 and silica. *Toxicol. Appl. Pharmacol.* **369**, 17–29. doi:10.1016/j.taap.2019.02.015
- Shukla, V. C., Higuera-Castro, N., Nana-Sinkam, P. and Ghadiali, S. N.** (2016). Substrate stiffness modulates lung cancer cell migration but not epithelial to mesenchymal transition. *J. Biomed. Mater. Res. A* **104**, 1182–1193. doi:10.1002/jbm.a.35655
- Wang, J., Sun, Q., Morita, Y., Jiang, H., Gross, A., Lechel, A., Hildner, K., Guachalla, L. M., Gompf, A., Hartmann, D. et al.** (2014). A differentiation checkpoint limits hematopoietic stem cell self-renewal in response to DNA damage. *Cell* **158**, 1444. doi:10.1016/j.cell.2014.08.033
- Wu, H., Yu, Y., Huang, H., Hu, Y., Fu, S., Wang, Z., Shi, M., Zhao, X., Yuan, J., Li, J. et al.** (2020). Progressive pulmonary fibrosis is caused by elevated mechanical tension on alveolar stem cells. *Cell* **180**, 107–121.e17. doi:10.1016/j.cell.2019.11.027
- Xia, Y., Ivanovska, I. L., Zhu, K., Smith, L., Irianto, J., Pfeifer, C. R., Alvey, C. M., Ji, J., Liu, D., Cho, S. et al.** (2018). Nuclear rupture at sites of high curvature compromises retention of DNA repair factors. *J. Cell Biol.* **217**, 3796–3808. doi:10.1083/jcb.201711161
- Xiaojun, W., Yan, L., Hong, X., Xianghong, Z., Shifeng, L., Dingjie, X., Xuemin, G., Lijuan, Z., Bonan, Z., Zhongqiu, W. et al.** (2016). Acetylated alpha-tubulin regulated by N-Acetyl-Seryl-Aspartyl-Lysyl-Proline (Ac-SDKP) exerts the anti-fibrotic effect in rat lung fibrosis induced by silica. *Sci. Rep.* **6**, 32257. doi:10.1038/srep32257
- Xu, Z., Schaedel, L., Portran, D., Aguilar, A., Gaillard, J., Marinkovich, M. P., Théry, M. and Nachury, M. V.** (2017). Microtubules acquire resistance from

- mechanical breakage through intraluminal acetylation. *Science* **356**, 328-332. doi:10.1126/science.aai8764
- Yang, F., Zhao, P. and She, M.** (1998). [The dynamic change of extracellular matrix in human coronary atherogenesis]. *Zhonghua Bing Li Xue Za Zhi* **27**, 177-181.
- Yeung, T., Georges, P. C., Flanagan, L. A., Marg, B., Ortiz, M., Funaki, M., Zahir, N., Ming, W., Weaver, V. and Janmey, P. A.** (2005). Effects of substrate stiffness on cell morphology, cytoskeletal structure, and adhesion. *Cell Motil. Cytoskeleton* **60**, 24-34. doi:10.1002/cm.20041
- Yong, K. W., Li, Y., Liu, F., Bin, G., Lu, T. J., Wan Abas, W. A., Wan Safwani, W. K., Pingguan-Murphy, B., Ma, Y., Xu, F. et al.** (2016). Paracrine effects of adipose-derived stem cells on matrix stiffness-induced cardiac myofibroblast differentiation via angiotensin II Type 1 receptor and Smad7. *Sci. Rep.* **6**, 33067. doi:10.1038/srep33067
- You, E., Huh, Y. H., Kwon, A., Kim, S. H., Chae, I. H., Lee, O.-J., Ryu, J.-H., Park, M. H., Kim, G.-E., Lee, J. S. et al.** (2017). SPIN90 depletion and microtubule acetylation mediate stromal fibroblast activation in breast cancer progression. *Cancer Res.* **77**, 4710-4722. doi:10.1158/0008-5472.CAN-17-0657
- Zeman, M. K. and Cimprich, K. A.** (2014). Causes and consequences of replication stress. *Nat. Cell Biol.* **16**, 2-9. doi:10.1038/ncb2897
- Zheng, H., Högberg, J. and Stenius, U.** (2017). ATM-activated autotaxin (ATX) propagates inflammation and DNA damage in lung epithelial cells: a new mode of action for silica-induced DNA damage? *Carcinogenesis* **38**, 1196-1206. doi:10.1093/carcin/bgx100